Supplementary References

1. Tokudome S, Sano M, Shinmura K, Matsuhashi T, Morizane S, Moriyama H, Tamaki K, Hayashida K, Nakanishi H, Yoshikawa N, Shimizu N, Endo J, Katayama T, Murata M, Yuasa S, Kaneda R, Tomita K, Eguchi N, Urade Y, Asano K, Utsunomiya Y, Suzuki T, Taguchi R, Tanaka H, Fukuda K. Glucocorticoid protects rodent hearts from ischemia/reperfusion injury by activating lipocalin-type prostaglandin D synthase-derived PGD2 biosynthesis. *J Clin Invest.* 2009;119:1477-1488.
2. Endo J, Sano M, Katayama T, Hishiki T, Shinmura K, Morizane S, Matsuhashi T, Katsumata Y, Zhang Y, Ito H, Nagahata Y, Marchitti S, Nishimaki K, Wolf AM, Nakanishi H, Hattori F, Vasiliou V, Adachi T, Ohsawa I, Taguchi R, Hirabayashi Y, Ohta S, Suematsu M, Ogawa S, Fukuda K. Metabolic remodeling induced by mitochondrial aldehyde stress stimulates tolerance to oxidative stress in the heart. *Circ Res.* 2009;105:1118-1127.
3. Endo J, Sano M, Fujita J, Hayashida K, Yuasa S, Aoyama N, Takehara Y, Kato O, Makino S, Ogawa S, Fukuda K. Bone marrow derived cells are involved in the pathogenesis of cardiac hypertrophy in response to pressure overload. *Circulation.* 2007;116:1176-1184.
4. Sun-Wada GH, Imai-Senga Y, Yamamoto A, Murata Y, Hirata T, Wada Y, Futai M. A proton pump ATPase with testis-specific E1-subunit isoform required for acrosome acidification. *J Biol Chem.* 2002;277:18098-18105.
5. Nakamura N, Yamamoto A, Wada Y, Futai M. Syntaxin 7 mediates endocytic trafficking to late endosomes. *J Biol Chem.* 2000;275:6523-6529.
6. Toyomura T, Oka T, Yamaguchi C, Wada Y, Futai M. Three subunit a isoforms of mouse vacuolar H(+)-ATPase. Preferential expression of the a3 isoform during osteoclast differentiation. *J Biol Chem.* 2000;275:8760-8765.
7. Nakamura N, Sun-Wada GH, Yamamoto A, Wada Y, Futai M. Association of mouse sorting nexin 1 with early endosomes. *J Biochem.* 2001;130:765-771.
8. Sun-Wada GH, Wada Y, Futai M. Lysosome and lysosome-related organelles responsible for specialized functions in higher organisms, with special emphasis on vacuolar-type proton ATPase. *Cell Struct Funct.* 2003;28:455-463.
9. Sano M, Tokudome S, Shimizu N, Yoshikawa N, Ogawa C, Shirakawa K, Endo J, Katayama T, Yuasa S, Ieda M, Makino S, Hattori F, Tanaka H, Fukuda K. Intramolecular control of protein stability, subnuclear compartmentalization, and coactivator function of peroxisome proliferator-activated receptor gamma coactivator 1alpha. *J Biol Chem.* 2007;282:25970-25980.

Online Figure I

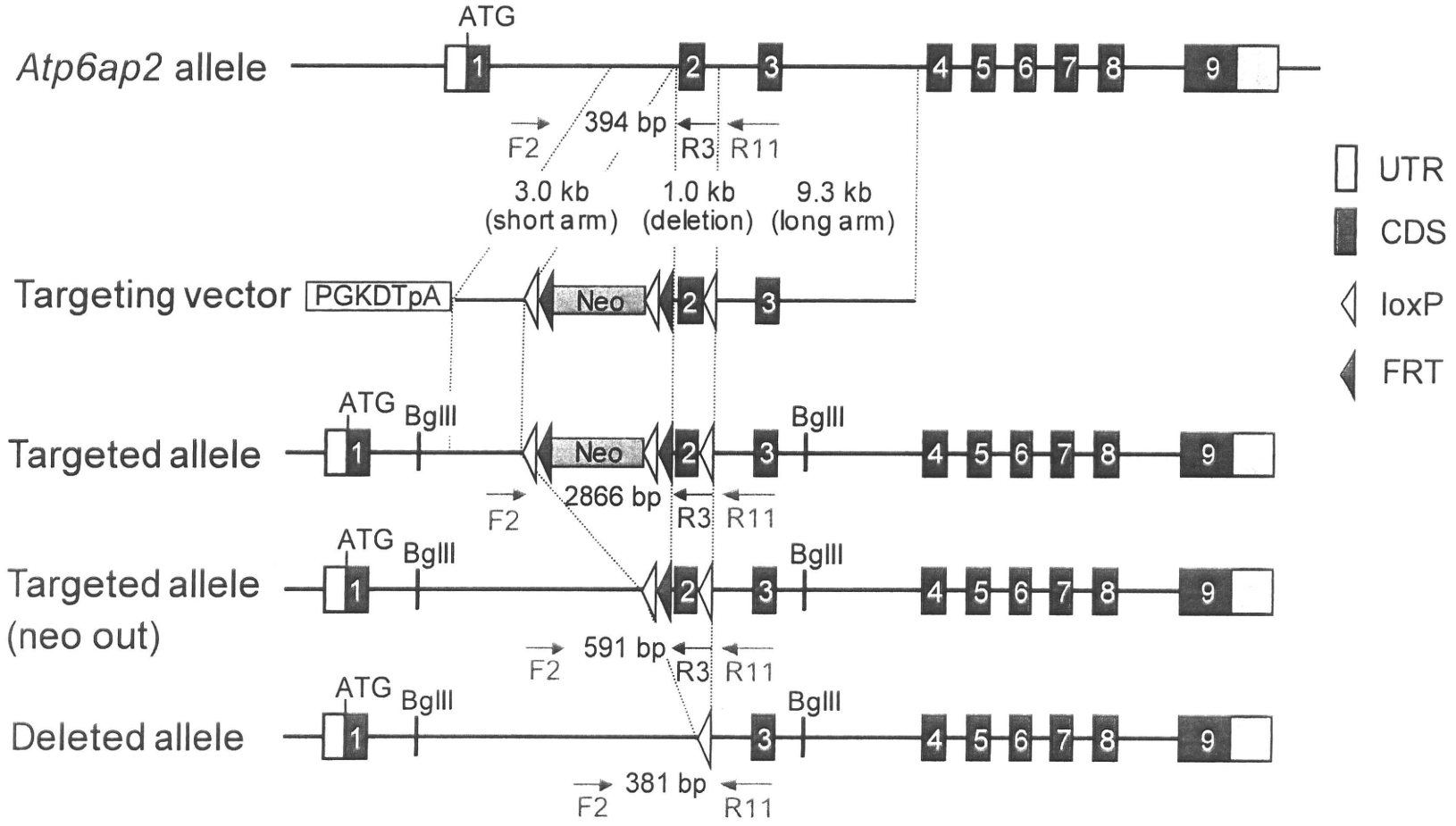

Online Figure II

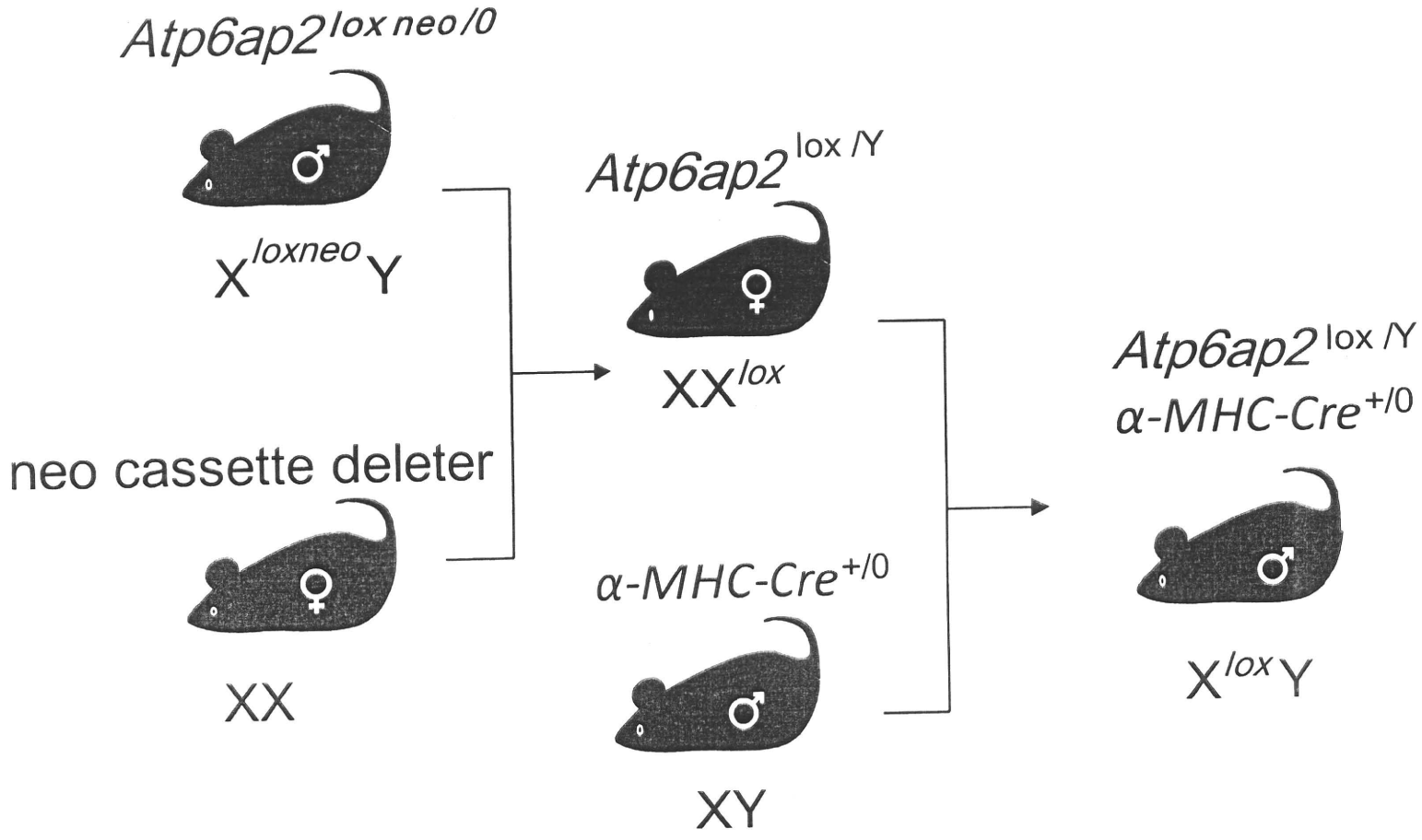

Online Figure III

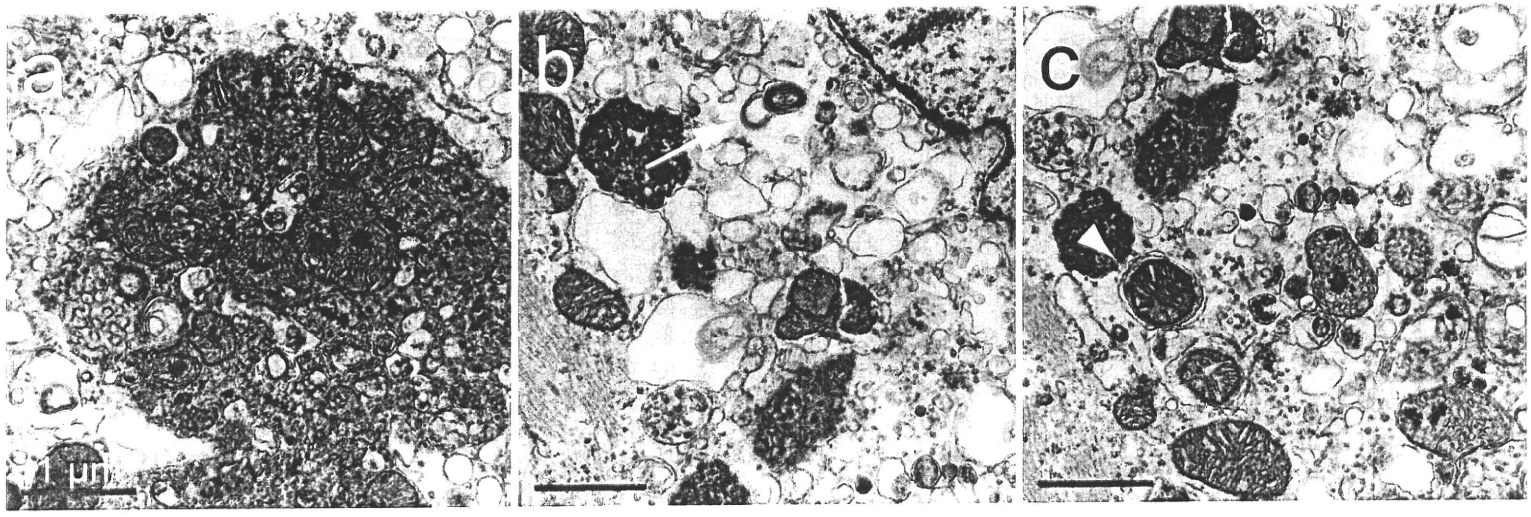

Online Figure IV

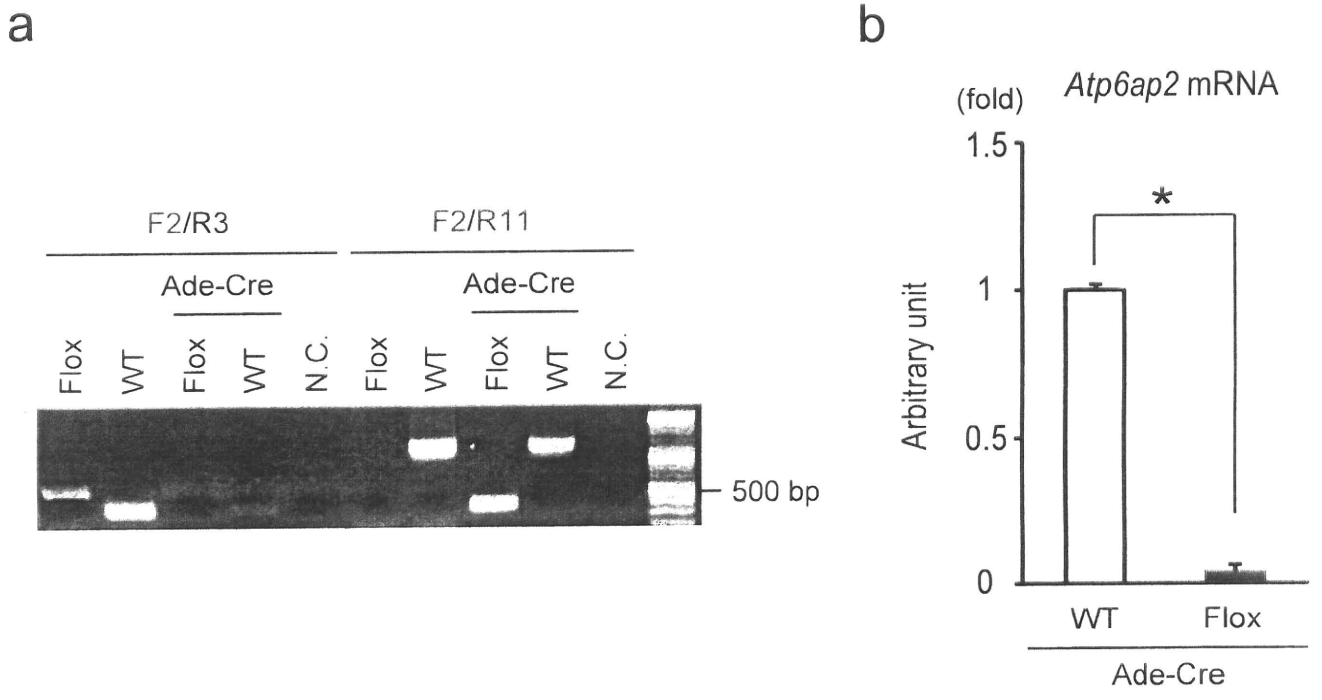

Online Figure V

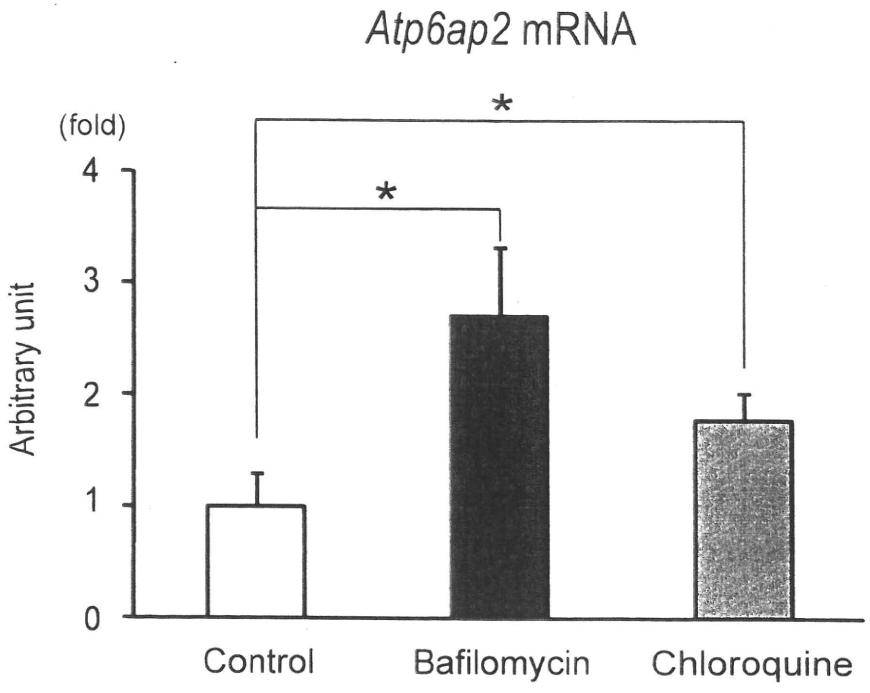

Generation of Induced Pluripotent Stem Cells from Human Terminally Differentiated Circulating T Cells

Tomohisa Seki,[1,7] Shinsuke Yuasa,[1,2,7] Mayumi Oda,[2] Toru Egashira,[1] Kojiro Yae,[1] Dai Kusumoto,[1] Hikari Nakata,[1] Shugo Tohyama,[1] Hisayuki Hashimoto,[1] Masaki Kodaira,[1] Yohei Okada,[2,3] Hiroyuki Seimiya,[4] Noemi Fusaki,[5,6] Mamoru Hasegawa,[5] and Keiichi Fukuda[1,*]

[1]Department of Cardiology
[2]Center for Integrated Medical Research
[3]Department of Physiology
Keio University School of Medicine, Tokyo 160-8582, Japan
[4]Division of Molecular Biotherapy, Cancer Chemotherapy Center, Japanese Foundation for Cancer Research, Tokyo 135-8550, Japan
[5]DNAVEC Corporation, Ibaraki 1-25-11, Japan
[6]PRESTO, JST, Saitama 332-0012, Japan
[7]These authors contributed equally to this work
*Correspondence: kfukuda@sc.itc.keio.ac.jp
DOI 10.1016/j.stem.2010.06.003

The direct reprogramming of somatic cells to produce induced pluripotent stem cells (iPSCs) is a prominent recent advance in stem cell biology (Takahashi and Yamanaka, 2006). Generation of iPSCs without genomic integration of extrinsic genes is highly desirable. Initially, human dermal fibroblasts were used to derive human iPSCs (hiPSCs) (Takahashi et al., 2007; Yu et al., 2007). However, recent studies have shown that other human somatic stem cells can be used (Aasen et al., 2008; Eminli et al., 2009; Kim et al., 2009; Ye et al., 2009). It is difficult to obtain human somatic stem cells, but human terminally differentiated circulating T cells (hTDCTCs) are readily available from peripheral blood. Here, we show that a combination of activated T cell cultivation and a temperature-sensitive mutated Sendai virus (SeV) that encodes human OCT3/4, SOX2, KLF4, and c-MYC allows the generation of hiPSCs easily, efficiently, and safely within a 1 month time frame.

Sampling of peripheral blood is one of the least invasive procedures performed routinely in clinics, and surplus peripheral blood samples are often left unused after clinical examinations. Among peripheral blood mononuclear cells (PBMCs), T cells can be readily cultured in vitro by means of a plate-bound anti-CD3 monoclonal antibody and recombinant (r)IL-2 (Desai-Mehta et al., 1996), and we used such an approach to expand hTDCTCs from peripheral blood samples. From 1 ml of whole blood, PBMCs were separated on a Ficoll gradient and then cultured with plate-bound anti-CD3 monoclonal antibody and rIL-2 (Figure 1A). Although PBMC fractions contain lymphocytes and monocytes, T cells are selectively cultured under these conditions. In culture, the number of activated T cells increased gradually but consistently. Five days after blood sampling, the cultured cells were morphologically identical to pure CD3-positive T cells collected by fluorescence-activated cell sorting (FACS) (Figure 1B). We used a whole-PBMC culture method because it is technically simpler than FACS, in which the sorted cells are frequently damaged by laser emission and the process of single-cell sorting.

To avoid transgene integration during iPSC generation, we used an SeV vector, which is a minus-strand RNA virus that is not integrated into the host genome and is not pathogenic for humans (Li et al., 2000). We used a temperature-sensitive mutated SeV vector in these experiments to reduce transgene expression and SeV residue in generated lines. This form of SeV vector generates weaker transgene expression and cannot proliferate at standard culture temperatures (data not shown). SeV can be efficiently transduced into human T cells and can express exogenous genes (Okano et al., 2003). We first introduced green fluorescent protein (GFP) into human T cells by SeV in a dose-dependent manner; toxicity for the infected cells was minimal at the virus dosages used (Figure 1C). To generate iPSCs from hTDCTCs, we used SeV to deliver multiple transgenes that encoded stem cell-specific transcription factors, such as *OCT3/4*, *SOX2*, *KLF4*, and *c-MYC*, into cells on day 6 of culture. Two days after gene introduction, the cells were replated onto feeder layers of SNL cells. On day 9, the cells were transferred to human ES cell (ESC) medium that contained 4 ng/ml bFGF. Within 3 weeks of infection, we identified a colony that resembled human ESCs (hESCs) among the T cell derivatives. On day 25, colonies that were larger and morphologically similar to hESC-like colonies were picked (Figure 1D). Of these initial colonies, which were identified by crystal violet staining, most were positive for alkaline phosphatase (ALP), which is a characteristic marker of stem cells (Figure 1E). T cells that had been transfected with SeV vectors carrying *OCT3/4, SOX2, KLF4,* and *c-MYC* were plated onto mitomycin C-treated SNL feeder cells at 5×10^4 cells per 10 cm dish. Around day 25 after blood sampling, the number of ALP-positive hESC-like colonies was counted and approximately 50 colonies were observed at MOI 20 (Figure 1E) (an efficiency of 0.1%). Moreover, the efficiency of iPSC colony generation was dependent upon the dosage of virus used for gene introduction (Figure 1F). We named these established T cell-derived iPSCs as "TiPS cells (TiPSCs)." After expansion, the cloned TiPSCs displayed typical hESC/iPSC morphology and had a normal karyotype (Figures S1A and S1B available online).

To confirm that the TiPSCs had the characteristics of typical ESC/iPSCs, we

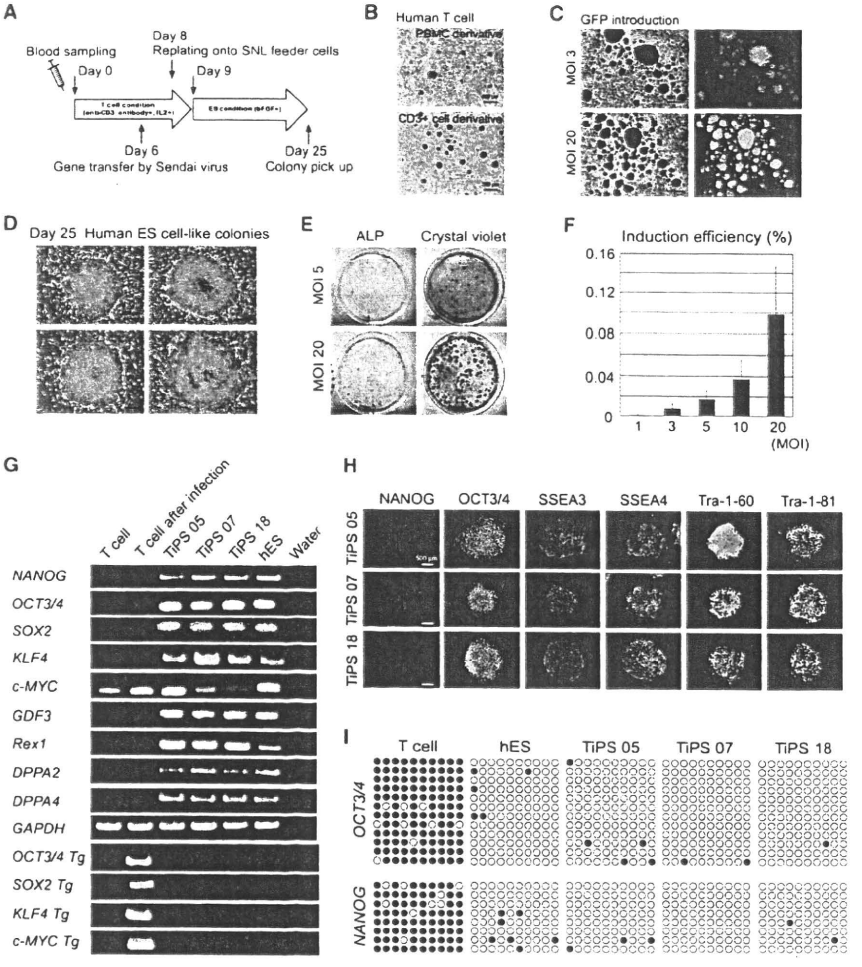

Figure 1. hTDCTCs-Derived iPSC Colonies

(A) Strategy used in the present study for reprogramming T cells.

(B) Morphologies of T cells derived from whole PBMCs or FACS-sorted T cells grown in the presence of CD3 antibody and rIL2.

(C) Efficient GFP introduction by SeV in T cells transfected at an MOI of 3 or MOI of 20.

(D) Typical ESC-like iPSC colonies on day 25 after blood sampling.

(E) Examples of 10 cm dishes stained for ALP on day 25, showing numerous ALP-positive colonies of T cells that were transfected at an MOI of 5 or MOI of 20.

(F) Numbers of ALP-positive colonies in relation to multiplicity of infection.

(G) RT-PCR analyses for the hESC marker genes *NANOG*, *OCT3/4*, *SOX2*, *KLF4*, *c-MYC*, *GDF3*, *REX1*, *DPPA2*, and *DPPA4* and the transgenes *OCT3/4*, *SOX2*, *KLF4*, and *c-MYC*.

(H) Immunofluorescence staining for pluripotency and surface markers (NANOG, OCT3/4, SSEA3, SSEA4, TRA-1-60, and TRA-1-81) in TiPS 05, 07, and 18. Scale bars represent 500 μm.

(I) Bisulfite sequencing analysis of the *NANOG* and *OCT3/4* promoter regions in peripheral T cells, hESCs, and hTiPSCs 05, 07, and 18. Each row of circles for a given amplicon represents the methylation status of the CpG dinucleotides in one bacterial clone for that region. Open circles represent unmethylated CpGs; closed circles represent methylated CpGs.

See also Figure S1 and Table S1.

examined stem cell marker expression. Reverse-transcription PCR (RT-PCR) analyses revealed that the TiPS 05, 07, and 18 clones expressed ESC marker transcripts for *NANOG*, *OCT3/4*, *SOX2*, *KLF4*, *c-MYC*, *GDF3*, *REX1*, *DPPA2*, and *DPPA4*. The original T cells also expressed *c-MYC* at a basal level, as previously reported (Douglas et al., 2001). In the TiPSCs, the *OCT3/4*, *SOX2*, *KLF4*, and *c-MYC* transgenes were lost after several passages (Figure 1G; Figure S1C). Immunostaining revealed that the TiPSCs expressed the Nanog, Oct3/4, SSEA3, SSEA4, Tra-1-60, and Tra-1-81 proteins (Figure 1H). High telomerase activity is also an important characteristic of iPSCs, and, appropriately, TiPSCs showed high levels of telomerase activity (Figure S1D). Another signature of iPSCs is epigenetic remodeling. We used bisulfite sequencing to examine the methylation status of the *NANOG* and *OCT3/4* promoters. T cells, which do not express *NANOG* or *OCT3/4*, showed mostly methylated CpGs in those promoters. hESCs, which do express *NANOG* and *OCT3/4*, showed unmethylated CpGs in those promoters. As in hESCs, the CpGs in these promoter regions were predominantly unmethylated in the TiPSCs (Figure 1I). These results suggest that SeV-mediated gene transfer successfully reprograms hTDCTCs.

Somatic recombination of T cell receptor (TCR) genes generates a diverse T cell repertoire that allows adaptation for antigen responses (Krangel, 2009). To confirm that the TiPSCs were derived from hTDCTCs, we analyzed TCR rearrangements. A hallmark of the TCR-β locus is developmentally ordered recombination, with Dβ-to-Jβ recombination preceding Vβ-to-DβJβ recombination. We performed capillary electrophoresis of the PCR products for the genomic DNA of the TCR-β regions. As a positive control, we used monoclonal T cells, which are derived from patients with lymphocyte malignancies and show a specific peak, because these T cells have only a single genetic variation in their TCR regions (Figure S2A). Peripheral T cells from people without lymphocytic diseases are polyclonal, with diverse genetic variations in their TCR rearrangements, and show a broad and low band without a specific peak. ESCs do not have TCR rearrangements and do not show a specific positive peak. The TiPS 05, 07, and 18 cell lines showed specific peaks for Dβ/Jβ recombination. TiPS 05 showed Vβ/Jβ2 recombination. TiPS 07 and TiPS 18 showed Vβ/Jβ1,2 recombination, albeit with different bands (Figure 2A). TCR rearrangement is specific for T cell development, so these results confirm that TiPSCs are derived from T cells. They also indicate that the TiPS 05, 07, and 18 lines originated from different T cells. We analyzed the rearrangement pattern of 10 independent TiPSCs and confirmed that every TiPSCs showed different rearrangement pattern (Figure S2A).

We also performed global gene expression analyses with DNA chips. Scatter plot analyses revealed global gene

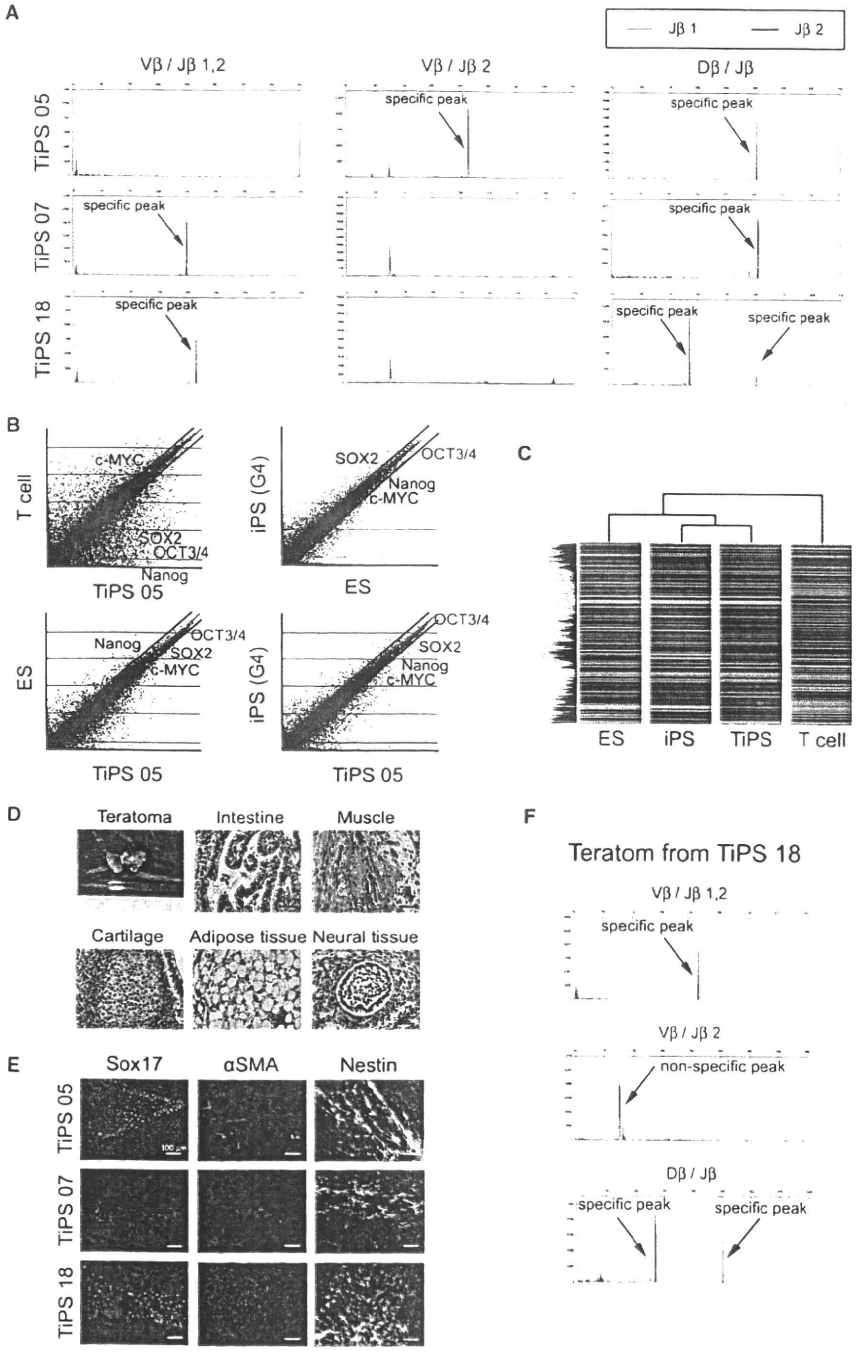

Figure 2. Detail Characterizations of TiPSCs

(A) Characterization of the TCR-β rearrangement by capillary electrophoresis. The green line is derived from the band for the Jβ1 gene, and blue line is derived from the band for the Jβ2 gene. TiPS 05 shows rearrangements of Vβ/Jβ2 and Dβ/Jβ. TiPS 07 shows rearrangements of Vβ/Jβ1,2 and Dβ/Jβ. TiPS 18 shows rearrangements of Vβ/Jβ1,2 and Dβ/Jβ.

(B) Scatter plots comparing the global gene expression profiles of T cells and TiPS cells, dermal fibroblast-derived iPSCs (G4) and ESCs, ESCs and TiPSCs, and dermal fibroblast-derived iPSCs (G4) and TiPSCs. The black lines indicate 2-fold differences in gene expression levels between the paired cell populations. The transcript expression levels are shown on a $\log_2$ scale. The expression levels of *NANOG*, *OCT3/4*, *SOX2*, and *c-MYC* are shown.

(C) Heat map analyses of hESCs, dermal fibroblast-derived iPSCs, TiPSCs, and the parental human T cells.

(D) Gross morphology, hematoxylin and eosin-stained representative teratomas derived from TiPS 05.

(E) Immunofluorescence staining for Sox17 (endodermal marker), αSMA (mesodermal marker), and Nestin (ectodermal marker) in each TiPSC-derived differentiated cell.

(F) Characterization of the TCR-β rearrangement for teratoma from TiPS 18.

See also Figure S2 and Table S2.

expression differences between peripheral T cells and TiPSCs. Comparison of hESCs and human dermal fibroblast-derived iPSCs, hESCs, and human TiPSCs (hTiPSCs), and dermal fibroblast-derived iPSCs and TiPSCs showed high levels of similarity (Figure 2B). Heat map analysis showed that the global gene expression profiles were overall similar in ESCs, dermal fibroblast-derived iPSCs, and TiPSCs, and different from T cells (Figure 2C). To further demonstrate the pluripotency of hTiPSCs, they were transplanted into the subcutaneous tissue of severe combined immunodeficient (SCID) mice. Six to eight weeks after injection, each TiPSC line tested gave rise to teratomas that contained derivatives of all three germ layers (Figure 2D; Figure S2B). We also examined the in vitro differentiation potential of TiPSCs. Each TiPSC line tested generated embryoid bodies that contained derivatives of all three germ layers (Figure 2E). These results indicate that hTiPSCs are pluripotent stem cells. Although it was reported that Trp53 null murine T cells could be reprogrammed into iPSCs (Hong et al., 2009), we have successfully reprogrammed wild-type human T cells. In our hands, the efficiency of conventional retrovirus-mediated gene transfer into wild-type human T cells was very low compared to SeV (data not shown). In our view, the efficiency of gene transfer is a major determining factor in successful iPSC generation.

With current technology, if iPSC-derived mature cells are transplanted into diseased patients, there is no good procedure for following their progeny, which could eventually form malignant or benign tumors. In animal models, several marker genes can be used to chart the progression and consequences of iPSC-derived mature cell transplantation, such as GFP and luciferase. However, it is not desirable to insert exogenous marker genes into the genomes of hiPSCs for clinical use. TiPSCs, however, already have a traceable genetic signature through TCR locus rearrangement. Consistent with this idea, teratomas derived from TiPSCs had

same signature as undifferentiated TiPSCs (Figure 2F; Figure S2C). Therefore, the descendents of TiPSCs can be identified by analyzing their TCR rearrangement patterns.

In conclusion, we have developed a minimally invasive method for hiPSC generation without genomic integration that uses low numbers of hTDCTCs from peripheral blood. This method has advantages for research into stem cell reprogramming, TCR rearrangement, immunologic disorders, and the development of genetic markers for future applications of regenerative medicine. TiPSCs may well be relatively easy to use in a clinical setting.

ACCESSION NUMBERS

The microarray data have been deposited in GEO and given the series accession number GSE22088.

SUPPLEMENTAL INFORMATION

Supplemental Information includes Supplemental Experimental Procedures, two figures, and two tables and can be found with this article online at doi:10.1016/j.stem.2010.06.003.

ACKNOWLEDGMENTS

This study was supported in part by research grants from the project for realization of regenerative medicine, the Ministry of Education, Science, and Culture, Japan, and by a grant from the New Energy and Industrial Technology Development Organization (NEDO). We thank Dr. Kyotaro Hirashima for technical assistance with TRAP assay. N.F. is an employee of DNAVEC Corporation and M.H. is a founder and shareholder of DNAVEC Corporation

Received: May 5, 2010
Revised: June 3, 2010
Accepted: June 5, 2010
Published: July 1, 2010

REFERENCES

Aasen, T., Raya, A., Barrero, M.J., Garreta, E., Consiglio, A., Gonzalez, F., Vassena, R., Bilic, J., Pekarik, V., Tiscornia, G., et al. (2008). Nat. Biotechnol. *26*, 1276–1284.

Desai-Mehta, A., Lu, L., Ramsey-Goldman, R., and Datta, S.K. (1996). J. Clin. Invest. *97*, 2063–2073.

Douglas, N.C., Jacobs, H., Bothwell, A.L., and Hayday, A.C. (2001). Nat. Immunol. *2*, 307–315.

Eminli, S., Foudi, A., Stadtfeld, M., Maherali, N., Ahfeldt, T., Mostoslavsky, G., Hock, H., and Hochedlinger, K. (2009). Nat. Genet. *41*, 968–976.

Hong, H., Takahashi, K., Ichisaka, T., Aoi, T., Kanagawa, O., Nakagawa, M., Okita, K., and Yamanaka, S. (2009). Nature *460*, 1132–1135.

Kim, J.B., Greber, B., Arauzo-Bravo, M.J., Meyer, J., Park, K.I., Zaehres, H., and Scholer, H.R. (2009). Nature *461*, 649–653.

Krangel, M.S. (2009). Curr. Opin. Immunol. *21*, 133–139.

Li, H.-O., Zhu, Y.-F., Asakawa, M., Kuma, H., Hirata, T., Ueda, Y., Lee, Y.-S., Fukumura, M., Iida, A., Kato, A., et al. (2000). J. Virol. *74*, 6564–6569.

Okano, S., Yonemitsu, Y., Nagata, S., Sata, S., Onimaru, M., Nakagawa, K., Tomita, Y., Kishihara, K., Hashimoto, S., Nakashima, Y., et al. (2003). Gene Ther. *10*, 1381–1391.

Takahashi, K., and Yamanaka, S. (2006). Cell *126*, 663–676.

Takahashi, K., Tanabe, K., Ohnuki, M., Narita, M., Ichisaka, T., Tomoda, K., and Yamanaka, S. (2007). Cell *131*, 861–872.

Ye, Z., Zhan, H., Mali, P., Dowey, S., Williams, D.M., Jang, Y.-Y., Dang, C.V., Spivak, J.L., Moliterno, A.R., and Cheng, L. (2009). Blood *114*, 5473–5480.

Yu, J., Vodyanik, M.A., Smuga-Otto, K., Antosiewicz-Bourget, J., Frane, J.L., Tian, S., Nie, J., Jonsdottir, G.A., Ruotti, V., Stewart, R., et al. (2007). Science *318*, 1917–1920.

Note Added in Proof

A manuscript has appeared online demonstrating isolation of iPSCs from peripheral blood, including a single line that showed evidence for both TCR-β and TCR-γ rearrangement by PCR (Kunisato, A., Wakatsuki, M., Shinba, H., Ota, T., Ishida, I., and Nagao, K. [2010]. Direct generation of induced pluripotent stem cells from human non-mobilized blood. Stem Cells Dev., in press. Published online May 24, 2010. 10.1089/scd.2010.0063).

Periostin advances atherosclerotic and rheumatic cardiac valve degeneration by inducing angiogenesis and MMP production in humans and rodents

Daihiko Hakuno,[1,2] Naritaka Kimura,[1,3] Masatoyo Yoshioka,[1] Makio Mukai,[4] Tokuhiro Kimura,[5] Yasunori Okada,[5] Ryohei Yozu,[3] Chisa Shukunami,[6] Yuji Hiraki,[6] Akira Kudo,[7] Satoshi Ogawa,[2] and Keiichi Fukuda[1]

[1]Department of Regenerative Medicine and Advanced Cardiac Therapeutics, [2]Cardiology Division, Department of Internal Medicine, [3]Department of Cardiovascular Surgery, [4]Division of Diagnostic Pathology, [5]Department of Pathology, Keio University School of Medicine, Tokyo, Japan. [6]Department of Cellular Differentiation, Institute for Frontier Medical Sciences, Kyoto University, Kyoto, Japan. [7]Department of Biological Information, Tokyo Institute of Technology, Kanagawa, Japan.

Valvular heart disease (VHD) is the term given to any disease process involving one or more of the heart valves. The condition can be congenital or acquired, for example as a result of atherosclerosis or rheumatic fever. Despite its clinical importance, the molecular mechanisms underlying VHD remain unknown. We investigated the pathophysiologic role and molecular mechanism of periostin, a protein that plays critical roles in cardiac valve development, in degenerative VHD. Unexpectedly, we found that periostin levels were drastically increased in infiltrated inflammatory cells and myofibroblasts in areas of angiogenesis in human atherosclerotic and rheumatic VHD, whereas periostin was localized to the subendothelial layer in normal valves. The expression patterns of periostin and chondromodulin I, an angioinhibitory factor that maintains cardiac valvular function, were mutually exclusive. In WT mice, a high-fat diet markedly increased aortic valve thickening, annular fibrosis, and MMP-2 and MMP-13 expression levels, concomitant with increased periostin expression; these changes were attenuated in periostin-knockout mice. In vitro and ex vivo studies revealed that periostin promoted tube formation and mobilization of ECs. Furthermore, periostin prominently increased MMP secretion from cultured valvular interstitial cells, ECs, and macrophages in a cell type–specific manner. These findings indicate that, in contrast to chondromodulin I, periostin plays an essential role in the progression of cardiac valve complex degeneration by inducing angiogenesis and MMP production.

Introduction

The prevalence of valvular heart disease (VHD) increases with age, reaching 13% in individuals 75 years of age or older (1). The morbidity associated with degenerative aortic valve disease is of global interest, given the aging of populations worldwide and the habitual consumption of food high in calories and cholesterol. Several lines of evidence (2–5) suggest that the mechanism of aortic valve degeneration is similar to that of atherosclerosis, namely, infiltration of inflammatory cells and accumulation of oxidized LDL within the valve, proliferation of valvular interstitial cells (VICs), extracellular matrix remodeling, and calcification. Based on this mechanism, prospective, randomized clinical trials of HMG CoA reductase inhibitors for preventing the progression of aortic valve stenosis have been performed, although the results are controversial (6, 7). As no preventive pharmacologic therapy for degenerative VHD has been proposed to date, further investigations into the underlying disease mechanisms and the development of novel therapies are warranted.

The previous studies conducted on VHD have largely been observational, immunohistologic, and in vitro studies (8–13). Although the onset of aortic valve stenosis has been reported in Smad6-deficient mice (14), in fibulin 4–deficient mice (15), and in humans with the *NOTCH1* mutation (16), the abnormality has primarily been observed during cardiac valve development. As avascular tissues, the cardiac valve complex and cartilage share common structural properties (17, 18). The cartilage and tendons are known to have unique angioinhibitory mechanisms (19), disruption of which results in angiogenesis and destruction of the joint, leading to arthritis (20). In contrast, angiogenesis and VEGF expression are increased in calcified aortic valves (21, 22). Previously, we showed that chondromodulin I (encoded by *Lect1*) and tenomodulin, angioinhibitory factors expressed in the cartilage and tendon, respectively, were expressed in the cardiac valves and chordae tendineae cordis (23, 24), respectively. Whereas chondromodulin I was expressed in the normal cardiac valves, its expression was diminished in areas of angiogenesis in the degenerated valves of human VHD. The absence of chondromodulin I results in angiogenesis and early stage aortic valve stenosis in mice, which indicates that cardiac valve degeneration is promoted by pathologic angiogenesis. The focal absence of tenomodulin is associated with angiogenesis and rupture of the chordae tendineae cordis.

Periostin (encoded by *Postn*) is a TGF-β–inducible, 90-kDa, secreted protein originally identified in mouse osteoblasts, in which it promotes adhesion and migration (25, 26). Periostin is detected as spliced isoforms and contains 4 repeats of the fasciclin domain, which shares homology with the *Drosophila* protein fasciclin I involved in neuronal cell-cell adhesion (27). In addition to

Conflict of interest: The authors have declared that no conflict of interest exists.

Citation for this article: *J Clin Invest* 2010;120(7):2292–2306. doi:10.1172/JCI40973.

the periosteum and periodontal ligament, periostin is expressed in cancer cells, vascular smooth muscle cells, fibroblasts, and wound-site blood vessels and participates in tumor angiogenesis, metastasis, and cell migration (28–31). In the heart, periostin is physiologically expressed in embryonic cardiac valves, while it is reexpressed abundantly in adult LV after pressure overload or myocardial infarction (32–37). Although heart size and cardiomyocyte number are unchanged at baseline in *Postn*$^{-/-}$ mice, LV remodeling and hypertrophy are attenuated without apparently affecting the proliferation of cardiomyocytes and cardiac fibroblasts, which suggests crucial effects of periostin on LV fibrosis and hypertrophy after cardiac insult (34, 35). Previous studies have clearly demonstrated the physiologic role of periostin in the cardiac valve and its critical involvement in cardiac valve maturation during development (38, 39). However, it remains unknown whether periostin plays any pathophysiologic role in adult valvular function.

During our investigation of degenerated human cardiac valves, we unexpectedly found that periostin was strikingly increased in patients with atherosclerotic and rheumatic VHD. This finding led us to hypothesize that periostin plays a distinct pathophysiologic role in degenerated cardiac valves. The present study demonstrates, for the first time to our knowledge, the involvement of periostin in the process of cardiac valve complex degeneration using human surgical specimens. We also investigated the pathophysiologic role of periostin in VHD using high-fat (HF) diet–induced degeneration of the cardiac valve complex and its rescue in *Postn*$^{-/-}$ mice. We further clarified the molecular mechanism by analyzing the in vitro effects of periostin on ECs, VICs, and engrafted macrophages.

Results

Periostin isoforms are specifically expressed in the cardiac valves and annuli of rodent hearts from the embryonic stage to adulthood. Because murine periostin is known to have 4 spliced isoforms within the C-terminal domain (Figure 1A, right), we initially determined the temporal and spatial expression patterns of the periostin isoforms in embryonic and adult mouse hearts. The RT-PCR analysis revealed that the periostin isoforms were first expressed in the E8.5 heart, and their levels increased thereafter (Figure 1A, left). Interestingly, the shift from the long isoform to the short isoform of periostin mRNA occurred in the postnatal heart. Western blot analysis revealed that the relative expression level of this protein in a heart decreased postnatally, probably as a result of its limited expression in valvular areas (Figure 1B). Furthermore, the short isoform was predominantly expressed in adult murine aortic valves, whereas the long isoform was mainly expressed in the mitral valves (Figure 1C).

Immunofluorescence staining with an anti-periostin antibody that recognizes both long and short isoforms showed that periostin was specifically expressed in the outflow tract and atrioventricular canal at E11.5 and in the cardiac valves and their annuli thereafter (Figure 1D). At 4 postnatal weeks, periostin expression appeared to be more localized to the subendothelial superficial layers of the cardiac valves and annuli.

Immunohistochemistry (IHC) of the adult rat cardiac valves confirmed that periostin was expressed in all 4 (aortic, mitral, pulmonary, and tricuspid) valves and in their annuli, in which the expression pattern of periostin was similar to that seen in murine valves (Figure 1E). These results indicate that periostin is expressed from E8.5 to adulthood in all 4 cardiac valves and that its expression is localized to the subendothelial superficial layers of the cardiac valves in adult rodent hearts.

Physiologic expression of periostin is localized primarily to the zona ventricularis/atrialis and zona fibrosa in adult human cardiac valves. Next, we investigated periostin expression in adult human normal cardiac valves obtained at autopsy. IHC revealed that periostin was expressed in the superficial layers of the normal aortic and mitral valves, whereas it was expressed throughout the murine embryonic valves (Figure 2, A and B, and Supplemental Figure 1; supplemental material available online with this article; doi:10.1172/JCI40973DS1). Of note, periostin was strongly expressed at the zona ventricularis side of the aortic valve and the atrialis side of the mitral valve, and to a lesser extent at the zona fibrosa of both, just beneath the ECs.

We also performed triple immunofluorescence staining for periostin and other components of the aortic valves. Interestingly, periostin was expressed in the subendothelial superficial layer, whereas chondromodulin I, an angioinhibitory protective factor in the cardiac valve (23), was expressed in the core layer of the cardiac valve (Figure 2C). Therefore, the expression patterns of these 2 proteins are mutually exclusive. The expression pattern of periostin did not coincide with that of either vWF or collagen I (Figure 2, D and E). Human cardiac valves consist of 3 distinct layers of extracellular matrix (fibrosa, spongiosa, and atrialis-ventricularis), and elastin is the predominant component of the atrialis and ventricularis (40). Indeed, the regions of periostin expression largely overlapped those of elastin (Figure 2F). Similar expression patterns were observed in the mitral valves (Supplemental Figure 2).

Periostin expression is strikingly upregulated and expanded in patients with atherosclerotic and rheumatic VHD. To investigate whether periostin is involved in the pathogenesis of VHD, we compared its expression profiles in normal human cardiac valves and in the cardiac valves of patients with VHD. Pathologic cardiac valves obtained by valvular replacement surgery, including atherosclerotic, rheumatic, and prolapse valves (n = 8, 9, and 4, respectively), were examined by IHC. Unexpectedly, we found not only that periostin expression was markedly elevated in the subendothelial superficial layer, but also that the area of periostin expression was expanded in the cardiac valves in patients with degenerative VHD, such as those with atherosclerotic or rheumatic valves. In the periostin-positive areas of the atherosclerotic valves, chondromodulin I expression was absent, whereas VEGF was upregulated and the small vessels were heavily infiltrated (Figure 3A). Similar findings were observed for rheumatic valves, whereas the periostin expression pattern did not show any significant changes in patients with mitral valve prolapse (Supplemental Figure 3).

Quantitative analysis revealed that the percentage of the expression area of periostin was increased 4.0-fold in patients with atherosclerotic and rheumatic valves, but not in those with valvular prolapse (Figure 3B). In patients with atherosclerotic or rheumatic valves, the chondromodulin I–positive areas were decreased to 25%, and the small vessel density, detected by vWF staining and VEGF expression, was markedly elevated, as we reported previously (23).

Western blot analysis revealed that the levels of periostin expression increased 6.1-fold and 3.2-fold in atherosclerotic and rheumatic VHD, respectively (Figure 3C). Concomitant with these increases in periostin, the levels of expression of α-SMA and collagen I were drastically increased in these patients.

Next, we examined the relationships between the areas of angiogenesis and periostin expression in these forms of VHD. IHC showed that neoangiogenesis occurred mainly at the zona atrialis/ventricularis and zona spongiosa in the mid-regions of the valves, especially in areas in which normal vWF expression was dimin-

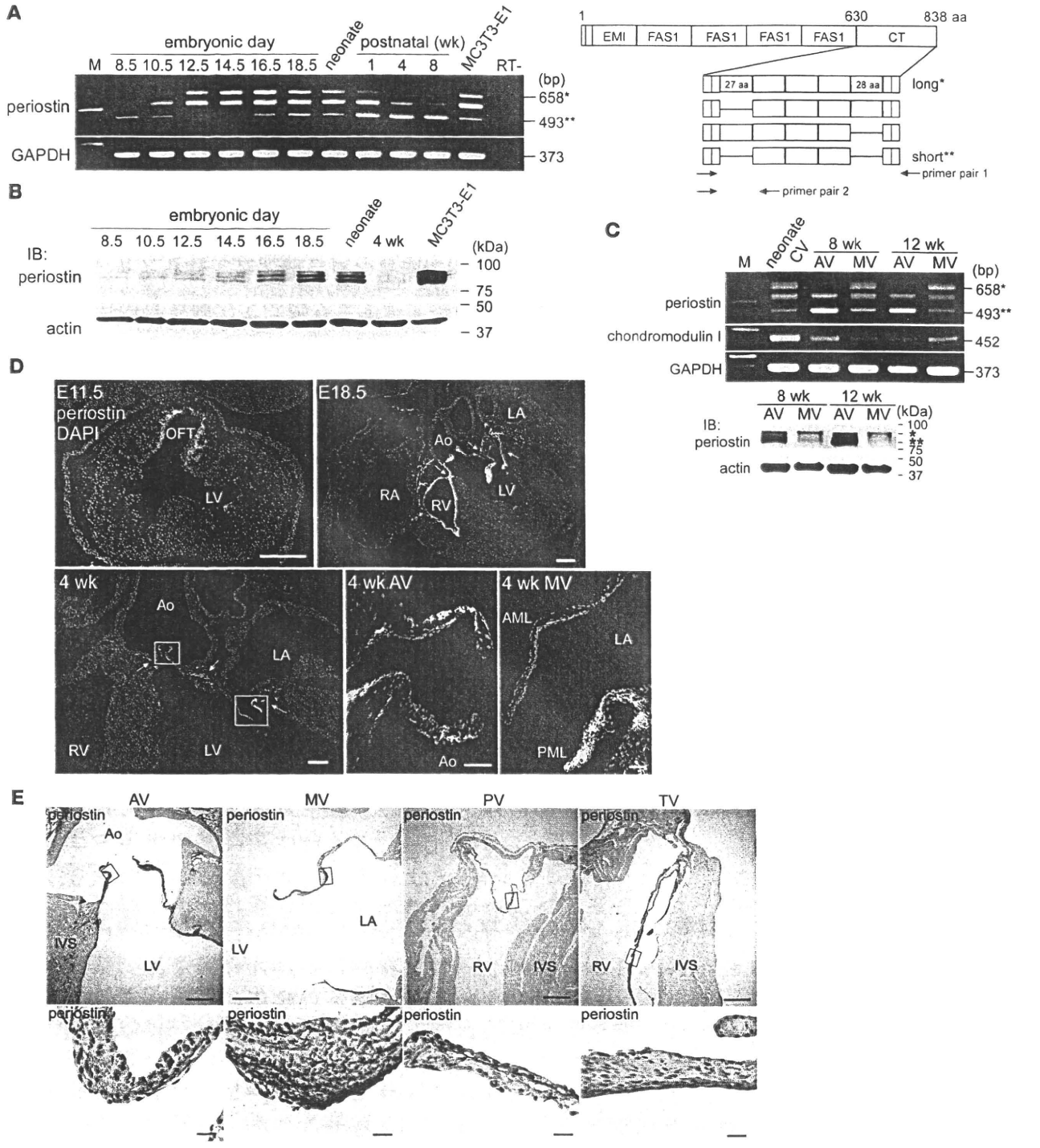

Figure 1

Periostin isoforms are specifically expressed in the cardiac valves and annuli of embryonic and adult rodent hearts. (**A** and **B**) RT-PCR (**A**) and Western blot (**B**) analyses of periostin isoforms in the mouse heart. The primer pair 1 for murine periostin (**A**, right) was used for PCR. Each box in the C-terminal (CT) domain represents an exon. Single and double asterisks represent the long and short periostin isoforms, respectively. Periostin was first detected in the hearts at E8.5, and the relative expression level of this protein decreased postnatally. MC3T3-E1 cells are a positive control. M, marker; FAS1, fasciclin I domain. (**C**) RT-PCR (top) and Western blot (bottom) analyses of the periostin isoforms in adult mouse cardiac valves (CV). AV, aortic valve; MV, mitral valve. (**D** and **E**) Immunostaining for periostin in the hearts of mice at E11.5 to 4 weeks of age (**D**) and in the heart of a 6-week-old rat (**E**). In **D**, periostin was specifically expressed in the outflow tract (OFT), cardiac valves, and annuli (arrows). In **E**, periostin (brown) was expressed in all 4 cardiac valves and their annuli. The boxed regions are shown at higher magnification. Note that periostin was localized to the subendothelial superficial layer of the adult cardiac valve. AML, anterior mitral leaflet; Ao, aorta; IVS, interventricular septum; LA, left atrium; PML, posterior mitral leaflet; PV, pulmonary valve; RA, right atrium; TV, tricuspid valve. Scale bars: 200 μm (**D**); 50 μm (**D**, higher magnification); 500 μm (**E**); 20 μm (**E**, higher magnification).

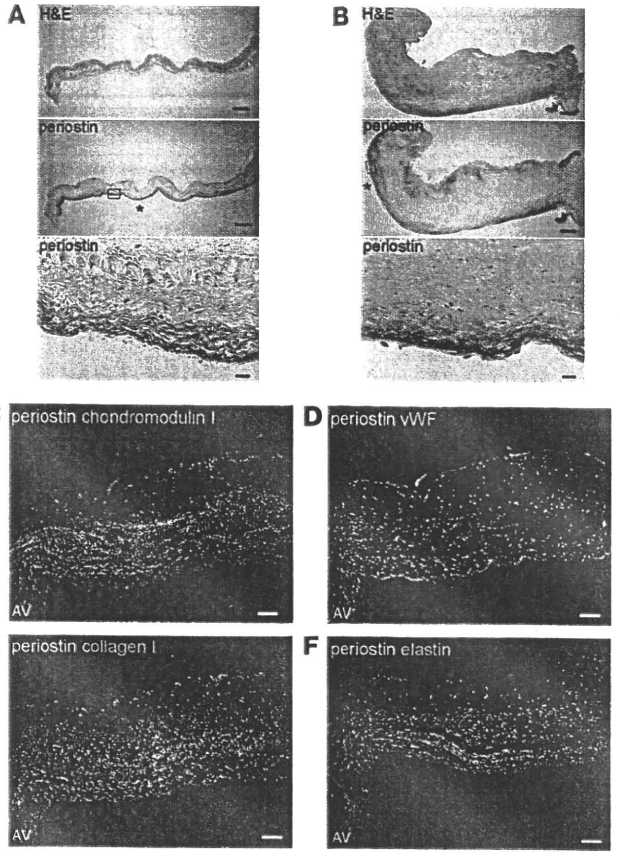

Figure 2

Physiologic expression of periostin is localized primarily to the zona ventricularis/atrialis and zona fibrosa in adult human cardiac valves. Representative, consecutive sections of normal human cardiac valves subjected to IHC (**A** and **B**) and triple-immunofluorescence staining (**C–F**). (**A** and **B**) IHC sections of the aortic valves (**A**) and mitral valves (**B**). The boxed regions in the periostin-stained sections are shown at higher magnification below. Prominent expression of periostin was observed at the ventricularis and atrialis sides (asterisks) and to a lesser extent at the zona fibrosa, just beneath the ECs. (**C–F**) Localization of periostin (green) and other components (red) in the normal aortic valves. Nuclei are stained blue. Since periostin was expressed in the subendothelial superficial layer and chondromodulin I in the core layer of the valve, the expression patterns of these proteins are mutually exclusive (**C**). The expression pattern of periostin overlapped with that of elastin (**F**), but not those of vWF and collagen I (**D** and **E**). Scale bars: 500 μm (**A** and **B**); 20 μm (**A** and **B**, higher magnification); 100 μm (**C–F**).

ished in the valve endocardium (Supplemental Figure 4A). We also found that periostin expression was specifically increased in the areas of neoangiogenesis in the degenerated valves (Supplemental Figure 4B). To identify the cell types that synthesize periostin in VHD, double immunofluorescence staining with periostin and vWF, α-SMA, vimentin, or the activated monocyte/macrophage marker CD14 was performed. Immunofluorescence staining revealed that periostin expression was increased in the interstitial tissues of the areas of angiogenesis, into which inflammatory cells and myofibroblasts had infiltrated (Figure 4A). Indeed, periostin was coexpressed with α-SMA, vimentin, and CD14 in these cells (Figure 4B). Immunofluorescence staining and Western blot analysis further confirmed that periostin was expressed and secreted from CD14-positive, cultured mouse BM-derived macrophages (Figure 4, C and D). These results indicate that periostin expression in degenerative atherosclerotic and rheumatic VHD, but not in prolapsed VHD, is completely different from its physiologic expression. In these forms of VHD, levels of periostin are markedly increased in the interstitial tissues of the newly formed small vessel areas, and periostin is secreted from the infiltrated inflammatory cells and myofibroblasts.

HF diet–induced thickening of the aortic valves and annuli is attenuated in Postn$^{-/-}$ mice. Our initial results led us to investigate whether the increased expression of periostin plays an essential role in cardiac valve degeneration or is merely an epiphenomenon. To resolve this issue, we generated *Postn*$^{-/-}$ mice of C57BL/6 strain (Figure 5A), and WT and *Postn*$^{-/-}$ mice at 12 weeks of age were fed either normal or HF diet for 4 months; C57BL/6 mice are the most atherosclerosis sensitive among mouse strains (41), and the HF regimen is known to cause significant thickening of their aortic valves, resulting in early-stage aortic valve stenosis (42). We found that the HF diet caused similar levels of obesity and hypercholesterolemia in WT and *Postn*$^{-/-}$ mice (Figure 5B).

We next performed 45-MHz echocardiography, which revealed that the HF diet produced high-echogenic areas in the aortic and mitral valve annuli in the HF diet–fed WT mice (Figure 5C). Moreover, the M-mode of echocardiography demonstrated that the aortic valve was apparently thickened in WT mice fed the HF diet compared with the normal diet. Surprisingly, the high-echogenic areas and aortic valve thickening were strongly attenuated in the HF diet–fed *Postn*$^{-/-}$ mice. Using quantitative analyses, we confirmed that the aortic valve thicknesses and echogenic areas of the annuli were significantly increased in HF diet–fed WT mice compared with WT mice fed normal diet, whereas these changes were strongly reduced in the HF diet–fed *Postn*$^{-/-}$ mice (Figure 5D). The wall thickness, internal diameter, and ejection fraction of the LV were unchanged in all the groups (Supplemental Figure 5). These results suggest that periostin is intrinsically involved in HF diet–induced degeneration of the cardiac valve complex.

HF diet–induced fibrosis and MMP expression in the cardiac valve complex are reduced in Postn$^{-/-}$ mice. To investigate further the role of periostin in valve degeneration, IHC and Western blot analysis were performed. Through quantitative analysis of the IHC sections, we confirmed that the HF diet increased the areas of periostin expression 2.2- to 2.5-fold in the aortic and mitral valve complexes of the WT mice (Figure 6, A and B). In addition, the areas of expression of vWF, collagen I, and α-SMA were increased in the HF diet–fed WT mice compared with WT mice fed normal diet, whereas expression levels of these proteins were markedly reduced in HF diet–fed *Postn*$^{-/-}$ mice.

The mitral valve complexes were then excised from the mice and subjected to Western blot analysis. The expression levels of periostin, collagen I, and α-SMA were significantly upregulated in the HF diet–fed WT mice and decreased in the HF diet–fed *Postn*$^{-/-}$ mice, confirming the IHC results (Figure 6C). It is well known that MMPs play critical roles in tissue remodeling and angiogenesis and are closely linked to the progression of atherosclerosis, aortic aneurysm, LV remodeling, and arthritis (43). Among the MMPs, MMP-13 is considered to fulfill the role of MMP-1 in rodents, which do not express the latter protein postnatally (44). Moreover, it has been reported previously that the levels of MMP-1, MMP-2, MMP-9, and MMP-13 are increased in the car-

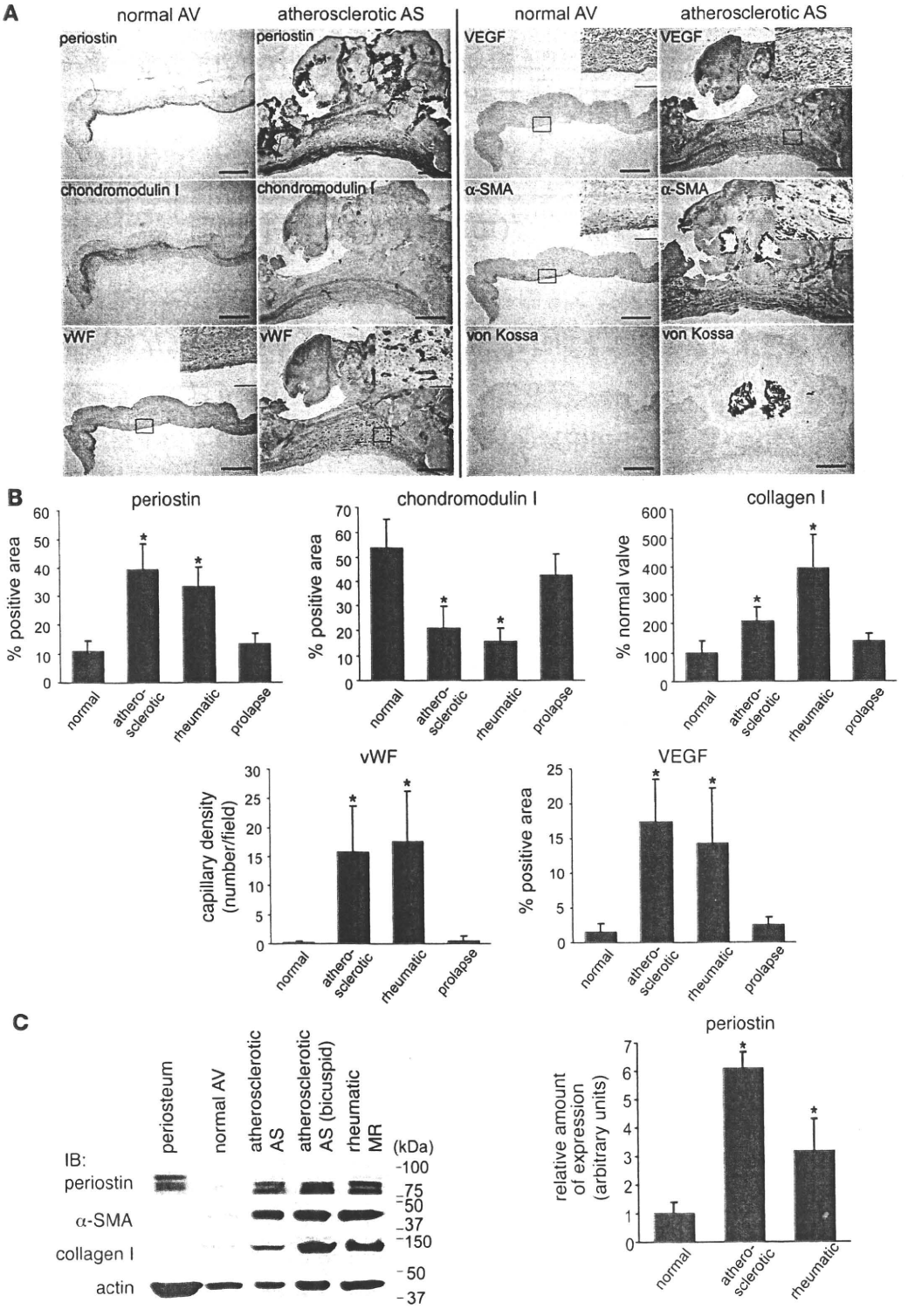

Figure 3

Periostin expression is strikingly upregulated and expanded in patients with atherosclerotic and rheumatic VHD. (**A**) Representative, consecutive IHC sections of normal aortic valves and atherosclerotic aortic valve stenosis. Boxed regions are shown at higher magnification in the insets. (**B** and **C**) Quantitative analyses of the expression of periostin, chondromodulin I, vWF, VEGF, α-SMA, and collagen I in normal valves and VHD valves, as measured by IHC (**B**) and Western blotting (**C**). The areas of expression of periostin, vWF, VEGF, α-SMA, and collagen I were strikingly expanded, whereas that of chondromodulin I was significantly reduced, in the atherosclerotic and rheumatic valves compared with the normal valves. The level of periostin expression was markedly increased in the atherosclerotic valves, and to a lesser extent in the rheumatic valves, as assessed by densitometric analysis of the Western blot. AS, aortic valve stenosis; MR, mitral valve regurgitation. Scale bars: 500 μm; 100 μm (insets). *$P < 0.05$ versus normal.

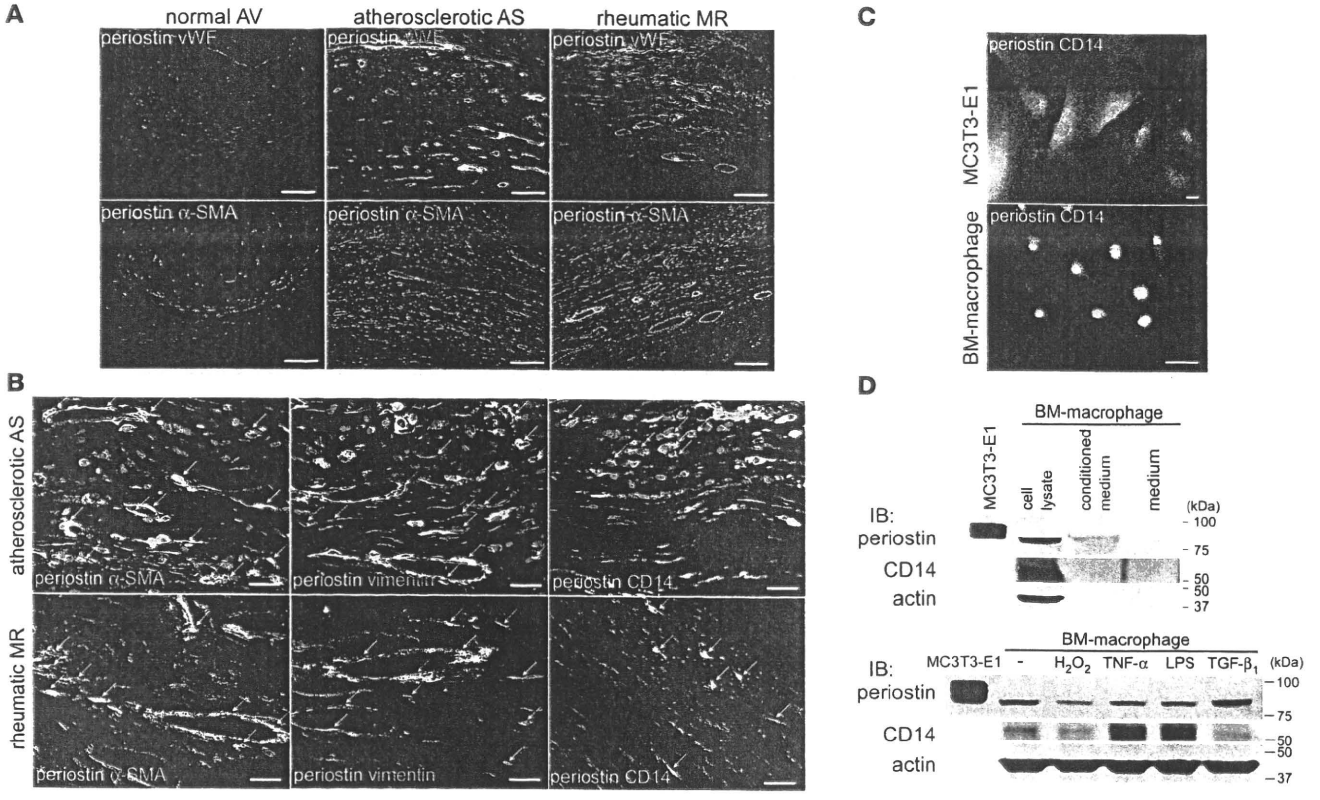

Figure 4

Periostin expression is specifically increased in the interstitial tissues of the neoangiogenesis areas in human VHD. (**A** and **B**) Triple-immunofluorescence staining for periostin (green) and vWF, α-SMA, vimentin, or the activated monocyte/macrophage marker CD14 (red). Nuclei are stained blue in **B**. Note that periostin was coexpressed with α-SMA, vimentin, and CD14 (arrows). (**C** and **D**) Double-immunofluorescence staining (**C**) and Western blot (**D**) analyses of periostin in cultured mouse BM-derived macrophages. MC3T3-E1 was used as a positive control for periostin expression. Periostin expression levels in macrophages treated with various stimuli for 24 hours are shown at the bottom of **D**. Periostin was expressed and secreted by the CD14-positive macrophages. Scale bars: 100 μm (**A**); 20 μm (**B** and **C**).

diac valves of patients with VHD (23, 45–47). We found that the expression levels of MMP-2 and MMP-13 significantly increased in HF diet–fed WT mice, whereas this increase was strongly reduced in HF diet–fed *Postn*$^{-/-}$ mice (Figure 6C). We also found modest calcification of the mitral valve annuli in HF diet–fed WT mice, but not in HF diet–fed *Postn*$^{-/-}$ mice (Supplemental Figure 6). We considered that the increase in the echogenic area of the annuli of the HF diet–fed WT mice may be caused by enhanced fibrosis and calcification. These results demonstrate that periostin mediates the HF diet–induced increases in fibrosis and MMP expression in the cardiac valve complex.

Periostin promotes angiogenesis in ECs both in vitro and ex vivo. To analyze further the function of periostin in cardiac valve degeneration, we performed in vitro experiments using ECs. As the differential roles of the periostin isoforms remained to be clarified, we collected the conditioned media of cultures of COS7 cells that expressed the long or short isoform of murine periostin as a result of being transfected with recombinant adenoviruses (Figure 7A), and the effects of these conditioned media on EC functions were examined. Previous studies have shown that periostin is expressed in aortic ECs, but not in valvular ECs, and that mesenchyme-specific cadherin 11 is expressed in valvular ECs, but not in aortic ECs, indicating phenotypic differences between valvular endocardial ECs and arterial ECs (48, 49). Using immunofluorescence staining and Western blotting, we found that cadherin 11, but not periostin, was expressed in human coronary artery ECs as well as in the ECs located in areas of neoangiogenesis in the stenotic aortic valves (Supplemental Figure 7). In contrast, periostin, but not cadherin 11, was expressed in aortic ECs. Therefore, human coronary artery ECs, rather than aortic ECs, were used in the in vitro angiogenesis assay.

Both the long and short periostin isoforms significantly and comparably promoted tube formation, migration, 3D lumen formation, and focal adhesion kinase (FAK) activation in ECs (Figure 7, B–E), in agreement with a previous report (50). Furthermore, periostin partially decreased the number of annexin V–positive apoptotic ECs induced by serum starvation and activated Akt without affecting EC proliferation (Figure 7, F–H, and Supplemental Figure 8).

The ex vivo aortic ring assay revealed that neoangiogenesis outward from the aortic roots and annuli in *Postn*$^{-/-}$ mice was strikingly inhibited compared with that in WT mice, and that periostin supplementation partially rescued this deficit (Supplemental Figure 9). Taken together, these results indicate that periostin itself promotes angiogenesis in ECs both in vitro and ex vivo and that the effects of the 2 periostin isoforms are comparable.

Periostin induces secretion of MMPs from VICs, ECs, and macrophages in vitro. Next, we investigated the effect of periostin on the functions of VICs, the predominant cell type in the cardiac valve. Cultured rat VICs, which stained positively for chondromodulin I and nega-

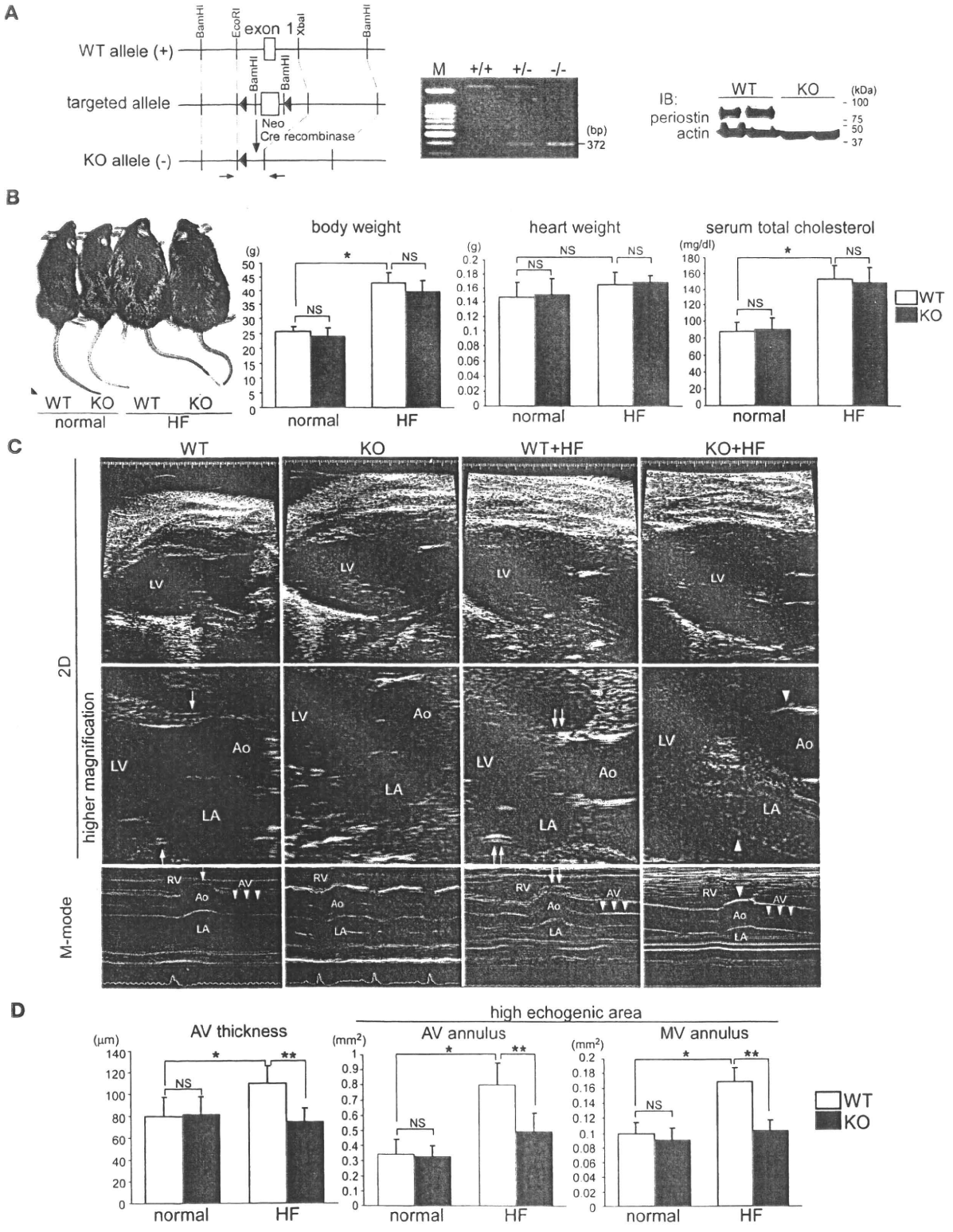
A
BamHI
EcoRI
exon 1
XbaI
BamHI
WT allele (+)
BamHI
BamHI
targeted allele
Neo
Cre recombinase
KO allele (-)
M +/+ +/- -/-
(bp)
372
IB:
WT KO
(kDa)
periostin
actin
100
75
50
37
B
body weight
heart weight
serum total cholesterol
(g)
(mg/dl)
NS
*
WT
KO
WT KO WT KO
normal HF
C
WT
KO
WT+HF
KO+HF
2D
higher magnification
M-mode
LV
Ao
LA
RV
AV
D
high echogenic area
AV thickness
AV annulus
MV annulus
(μm)
(mm²)
**

Figure 5
HF diet–induced thickening of the aortic valves and annuli is attenuated in *Postn*$^{-/-}$ mice. (**A**) Generation of *Postn*$^{-/-}$ mice. Schema of the strategy used for targeting the first exon of the murine *Postn* gene. Genotyping of mouse offspring was performed by PCR of tail-DNA samples. The primer pair used is indicated by arrows in the schema. Also shown is Western blot analysis of the periostea in the WT and *Postn*$^{-/-}$ (KO) mice. (**B**) Appearance of mice fed normal diet or HF diet for 4 months. The HF diet caused similar levels of obesity and hypercholesterolemia in both WT and *Postn*$^{-/-}$ mice. (**C** and **D**) Representative images (**C**) and quantitative analyses of the aortic valve thicknesses and echogenic areas of the annuli (**D**), as assessed by 45-MHz echocardiography. In **C**, images were taken at the diastolic phase using the 2D mode, and at the level of the aortic valve using the M-mode of the left parasternal long axis view. The echogenic areas of the aortic and mitral valve annuli greatly increased in the HF diet–fed WT mice (double arrows) compared with those in the WT mice (arrows). These changes were reduced in the HF diet–fed *Postn*$^{-/-}$ mice (arrowheads). Furthermore, the HF diet–induced thickening of the aortic valves was significantly attenuated in the HF diet–fed *Postn*$^{-/-}$ mice (triple arrowheads). Original magnification, ×10; ×40 (higher magnification). $^{*}P < 0.05$ versus WT; $^{**}P < 0.05$ versus HF diet–fed *Postn*$^{-/-}$.

tively for acetylated LDL (Figure 8A), were prepared as described previously (23). Periostin neither affected VIC proliferation (Supplemental Figure 10A) nor reduced serum starvation–induced apoptosis (Supplemental Figure 10B). Interestingly, however, Western blot analysis revealed that periostin strikingly increased the secretion of MMP-2 and MMP-13 from VICs, whereas it did not affect MMP-9 secretion (Figure 8B). RT-PCR analysis showed that periostin strongly induced the transcription of *Mmp13*, but not that of *Mmp2* (Figure 8C). Moreover, it significantly stimulated the secretion of MMP-2 and MMP-9 from ECs and cultured BM-derived macrophages, respectively (Figure 8, D and E), suggestive of cell type–specific induction of MMPs by periostin. These results demonstrate that periostin promotes the secretion of MMPs from VICs, ECs, and macrophages in vitro. Our in vitro findings strongly support the notion that periostin plays a critical role in promoting cardiac valve complex degeneration.

Periostin and chondromodulin I do not cross-regulate each other in the cardiac valves. The reciprocal expression patterns and functions of periostin and chondromodulin I led us to consider whether these proteins cross-regulate each other in the cardiac valves. To examine this possibility, the cardiac valves of *Postn*$^{-/-}$ and *Lect1*$^{-/-}$ mice (23) were examined for chondromodulin I and periostin expression, respectively, using IHC and Western blot analysis. We found that chondromodulin I expression was not altered in the valves of HF diet–fed WT and *Postn*$^{-/-}$ mice (Supplemental Figure 11A). Conversely, periostin expression was unchanged in the valves and annuli of the WT and *Lect1*$^{-/-}$ mice (Supplemental Figure 11, B and C). Moreover, periostin stimulation affected neither the transcription nor the translation of chondromodulin I in rat VICs in vitro (Supplemental Figure 11D). These results indicate that periostin and chondromodulin I do not cross-regulate each other in the cardiac valves.

Discussion

Previous studies showed that periostin plays an important role in cardiac valve development (38, 39). However, the results of the present study demonstrate that periostin has a distinct role in the progression of cardiac valve degeneration in atherosclerotic and rheumatic VHD. Periostin expression was localized to the subendothelial superficial layer of normal cardiac valves and annuli in adult human hearts, while it was greatly increased in the areas of neoangiogenesis in the degenerated valves of patients with VHD. Moreover, we also found that HF diet induced degeneration of the cardiac valve complex in WT mice, whereas this degeneration was markedly rescued in *Postn*$^{-/-}$ mice via the prevention of fibrosis and MMP expression. Finally, we found that periostin affected the functions of major cellular components of the degenerated valves, in that it not only promoted angiogenesis in ECs, but also increased the secretion of MMPs from VICs, ECs, and engrafted macrophages in vitro. The reciprocal expression patterns and functions of periostin and chondromodulin I clearly define the degenerative role of periostin and the protective role of chondromodulin I in the progression of degenerative VHD.

A recent study reported that periostin expression was decreased in the valves of infants with congenital bicuspid aortic valve stenosis (39). Moreover, the authors revealed that *Postn*$^{-/-}$ mice exhibited truncated and disorganized cardiac valves. That study showed that decreased physiologic expression of periostin during the developmental stage resulted in congenital valve deformities. In contrast, we focused for the first time to our knowledge on the expression and role of periostin in adult-acquired VHD, particularly in degenerative atherosclerotic and rheumatic VHD. We found that periostin was pathologically overexpressed in these forms of VHD, in which it was abundantly secreted by infiltrated inflammatory cells and myofibroblasts. It is possible that these myofibroblasts are recruited from circulating fibrocytes, as it has previously been shown that bone marrow–derived hematopoietic stem cells contribute to the adult cardiac VIC population (51) and that peripheral blood fibrocytes originating from hematopoietic stem cells or CD14-positive peripheral blood monocytes can differentiate into myofibroblasts in several tissues (52). In these instances, the origins of the periostin-producing cells were completely dissimilar to those of the cells involved in its physiologic expression. In contrast, the expression levels of periostin were significantly lower, and those of collagen I were significantly higher, in the valves of rheumatic VHD than in those of atherosclerotic VHD. Given these findings, it might be appropriate to describe rheumatic VHD as a phenotype of accelerated formation and reorganization of extracellular matrices rather than as a phenotype of degeneration.

We also demonstrated that periostin had tube-forming and migratory activities in ECs both in vitro and ex vivo, and we confirmed that these activities were mediated by the activation of FAK and Akt, which indicated that periostin has angiogenic activity. It is well known that the normal cardiac valve is an avascular tissue, whereas the degenerated valve contains numerous small vessel infiltrations. We believe that periostin upregulation in the degenerated valves is critical for small vessel formation and for collaboration with other angiogenic factors (53). In support of our observations, the angiogenic activity of periostin has been implicated in tumor angiogenesis (29, 50, 54). Although the precise periostin-mediated angiogenic mechanisms within the valves are not elucidated in the present study, we demonstrated that neoangiogenesis occurred mainly in the zona atrialis/ventricularis and spongiosa in the mid-regions of the valves, particularly at sites in which the normal structure of the valve endocardium is disrupted. Therefore, periostin may enhance the recruitment of circulating endothelial progenitor cells by promoting their adhesion and migration into the valves, or it might enhance the penetration of the microvessels from the annulus region or roots into the leaflets.

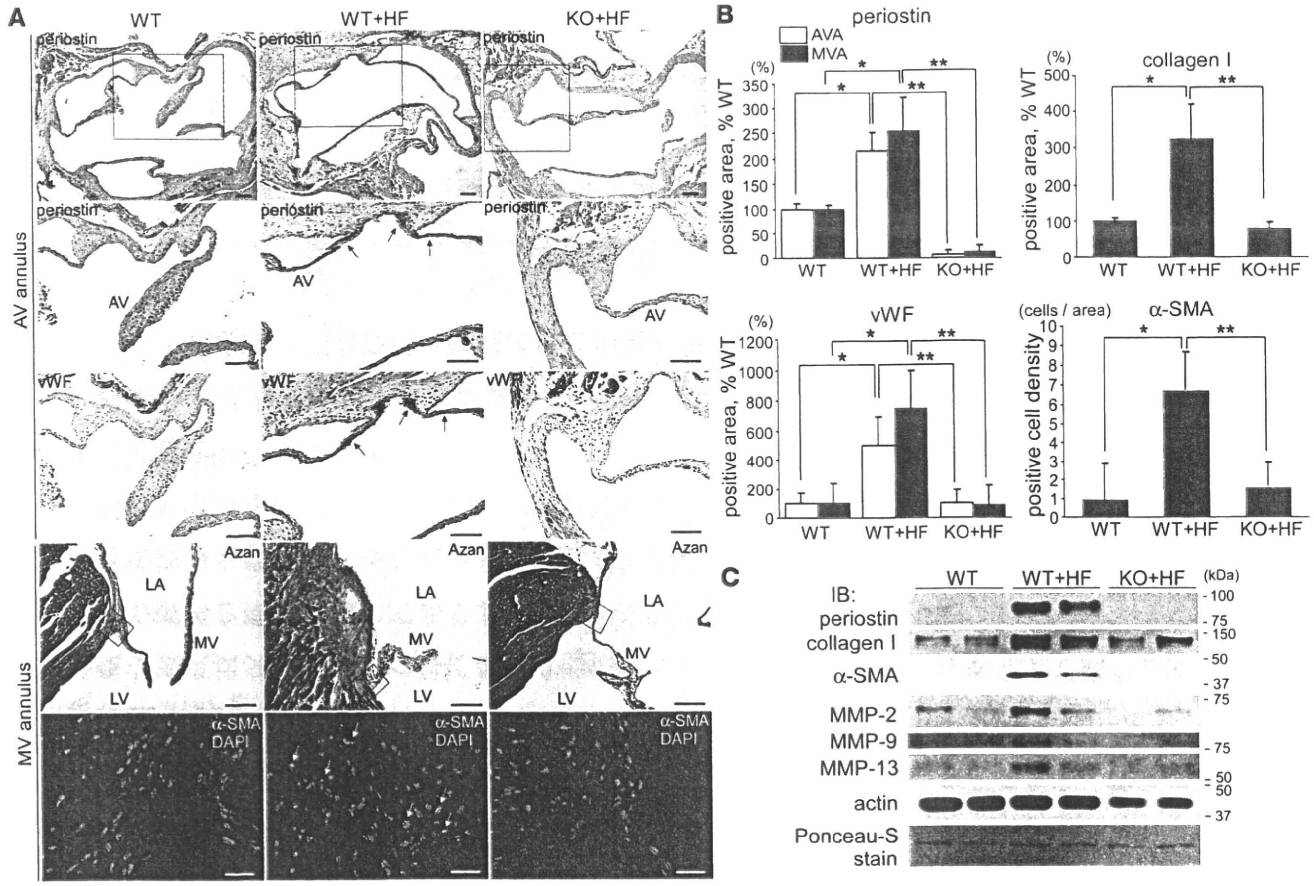

Figure 6

HF diet–induced fibrosis and MMP expression in the cardiac valve complex are reduced in *Postn*$^{-/-}$ mice. (**A–C**) Representative IHC sections (**A**), quantitative analyses of the expression areas (**B**), and Western blot analysis (**C**) of the cardiac valve complexes in WT and *Postn*$^{-/-}$ mice. (**A**) Horizontal sections of AV annuli and longitudinal sections of MV annuli are shown. The boxed regions in the periostin-stained sections are shown at higher magnification immediately below, and the boxed regions in the Azan-stained sections are shown as α-SMA immunofluorescence below. The areas of expression of periostin, vWF, and α-SMA and the Azan-stained areas were markedly expanded in the HF diet–fed WT mice (arrows), whereas these changes were reduced in the HF diet–fed *Postn*$^{-/-}$ mice. (**B**) The areas of expression in the aortic valve annulus (AVA) and mitral valve annulus (MVA) are shown as percentages relative to WT mice. (**C**) Murine mitral valves with annuli were excised and subjected to Western blot analysis. The expression levels of periostin, collagen I, α-SMA, MMP-2, and MMP-13 were greatly increased in the HF diet–fed WT mice and reduced in HF diet–fed *Postn*$^{-/-}$ mice. Scale bars: 100 μm; 20 μm (α-SMA immunofluorescence). $^{*}P < 0.05$ versus WT; $^{**}P < 0.05$ versus HF diet–fed *Postn*$^{-/-}$.

MMPs are critically involved not only in appropriate embryonic development, but also in the progression of various degenerative diseases. Previously, we reported that MMP-1, MMP-2, MMP-9, and MMP-13 were overexpressed in areas of neoangiogenesis in patients with degenerative VHD, although the precise mechanisms were unknown (23). The present study clearly shows that periostin increased secretion of MMP-2, MMP-9, and MMP-13 from VICs, ECs, and cultured macrophages in a cell type–specific manner. Moreover, periostin upregulated MMP-2 expression in VICs by posttranscriptional mechanisms, possibly by inhibiting MMP-2 binding to the cell surface or by its degradation, as previously reported (55–58). MMP-2 can activate MMP-9 and MMP-13 (43). MMP-13 is secreted from stimulated synoviocytes and fibroblasts, as well as from tumor cells, and plays a critical role in degenerative bone diseases, such as osteoarthritis and rheumatoid arthritis (59, 60). As the cardiac valvular complex and cartilage have common structural features, it is conceivable that periostin induces MMP-13 expression in VICs. To our knowledge, this is the first report to describe the induction of MMPs by periostin. Periostin has been shown to promote collagen fibrillogenesis in myocardial infarction and the cardiac valve explants (37, 61), whereas MMPs are involved in the initiation and progression of collagen fibril growth (62). Therefore, we assume that the activation of MMPs mediates, at least in part, the effects of periostin on collagen fibrillogenesis and angiogenesis. A recent study has indicated that periostin is induced during LV remodeling after cardiac injury without affecting cardiac fibroblast proliferation (35). Interestingly, we also found that periostin was reexpressed during cardiac valve degeneration without affecting VIC proliferation, which suggests that it regulates cardiac pathologic remodeling via common biological mechanisms, including those that involve MMPs. Taken together, our data demonstrate that periostin causes cardiac valve complex degeneration by promoting angiogenesis and production of MMPs, which in turn facilitate the infiltration of periostin-

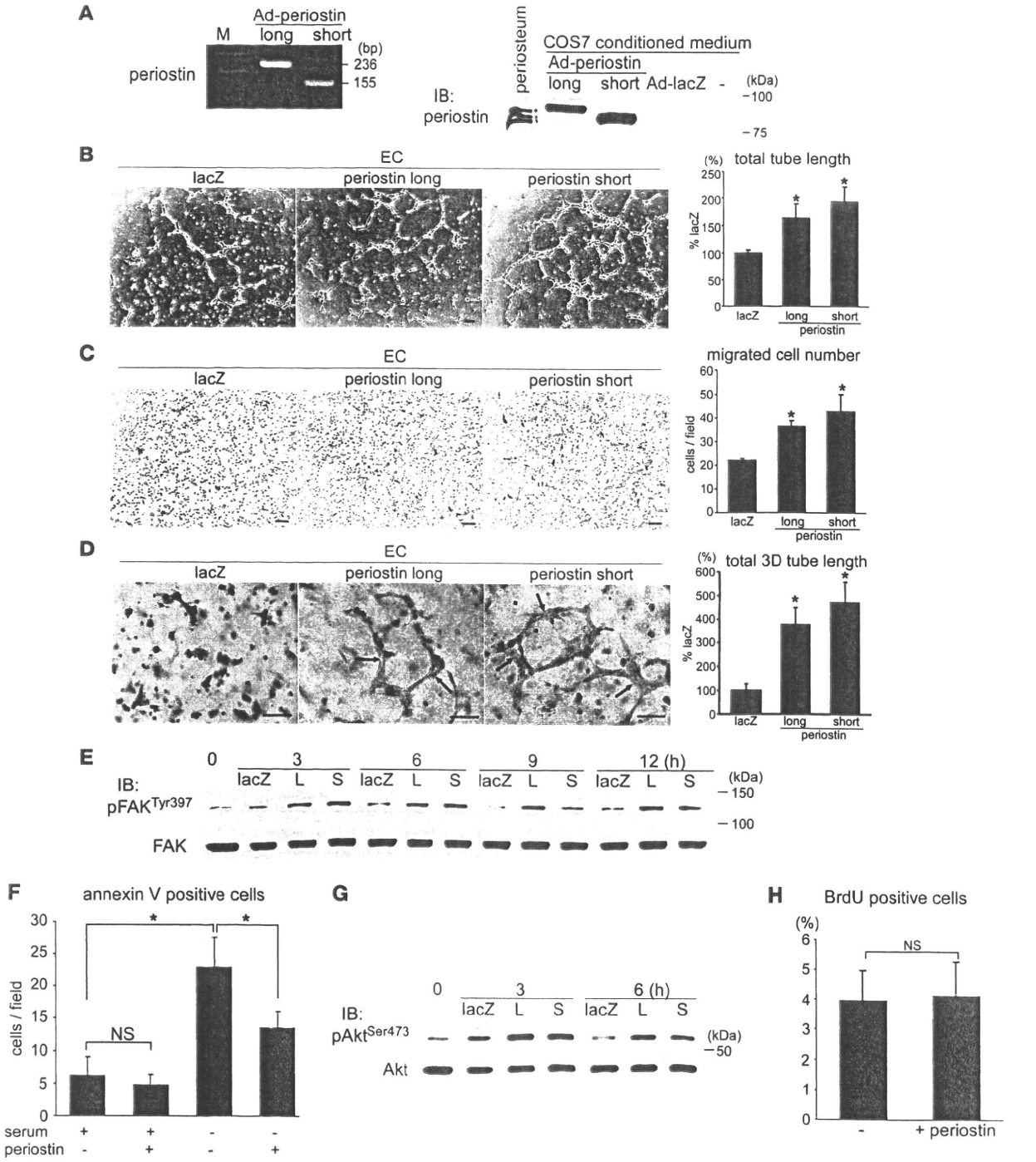

Figure 7

Periostin isoforms comparably promote angiogenesis in ECs in vitro. (**A**) Generation of isoform-specific murine periostin. Left: PCR of DNA from adenoviruses that contain the long or short periostin isoform. Primer pair 2 (see Figure 1A) was used. Right: Western blot analysis of COS7 cell-conditioned media. COS7 cells were infected with adenoviruses (Ad) that carried the long or short isoform of periostin or LacZ, and the conditioned media were collected. (**B–D**) Tube formation assay (**B**), migration assay (**C**), and 3D vasculogenesis assay (**D**) for human coronary artery ECs. ECs were stimulated with COS7-conditioned media, prepared as described in **A**. Both the long and short isoforms of periostin significantly and comparably promoted tube formation and mobilization. The formed luminal structures are shown by arrows in **D**. Scale bars: 100 μm. $^*P < 0.05$ versus LacZ. (**E**) FAK activation in ECs by periostin stimulation. L, long periostin isoform; S, short periostin isoform. (**F**) Apoptosis assay for ECs. ECs were stimulated with or without the long isoform of periostin either in 10% FBS or under serum starvation conditions for 24 hours. Periostin significantly inhibited serum starvation–induced EC apoptosis. $^*P < 0.05$. (**G**) Periostin-induced Akt activation in ECs. (**H**) BrdU incorporation assay for ECs stimulated with or without the long isoform of periostin. Periostin did not affect EC proliferation.